nature neuroscience

K-ATP channels in dopamine substantia nigra neurons control bursting and novelty-induced exploration

Julia Schiemann[1], Falk Schlaudraff[2], Verena Klose[1], Markus Bingmer[3], Susumu Seino[4], Peter J Magill[5], Kareem A Zaghloul[6], Gaby Schneider[3], Birgit Liss[2,7] & Jochen Roeper[1,7]

Phasic activation of the dopamine (DA) midbrain system in response to unexpected reward or novelty is critical for adaptive behavioral strategies. This activation of DA midbrain neurons occurs via a synaptically triggered switch from low-frequency background spiking to transient high-frequency burst firing. We found that, in medial DA neurons of the substantia nigra (SN), activity of ATP-sensitive potassium (K-ATP) channels enabled NMDA-mediated bursting *in vitro* as well as spontaneous *in vivo* burst firing in anesthetized mice. Cell-selective silencing of K-ATP channel activity in medial SN DA neurons revealed that their K-ATP channel–gated burst firing was crucial for novelty-dependent exploratory behavior. We also detected a transcriptional upregulation of K-ATP channel and NMDA receptor subunits, as well as high *in vivo* burst firing, in surviving SN DA neurons from Parkinson's disease patients, suggesting that burst-gating K-ATP channel function in DA neurons affects phenotypes in both disease and health.

The DA system is activated by unexpected rewards, novelty and other salient stimuli, and is essential for flexible control of behavioral strategies. DA midbrain neurons integrate synaptically relayed sensory inputs and other signals to select and learn motor programs[1,2]. Distinct subpopulations of DA midbrain neurons innervate different areas of the cortex and basal ganglia[3,4] that control, learn, prioritize and update motor decisions in a context- and reward-dependent manner. In humans, high-resolution functional magnetic resonance imaging has identified distinct DA midbrain regions that are preferentially activated by either reward or novelty[5]. However, the cellular and molecular bases of differential signaling in distinct DA subpopulations are unknown.

Dopamine midbrain neurons respond to novel or reward-predicting sensory cues and to unexpected rewards with a switch from low-frequency firing to phasic burst firing at higher frequencies[2]. Some DA neuron subpopulations also burst in response to aversive or salient stimuli[1], whereas others generate burst discharges as start and stop signals of learned action sequences[6]. DA neuron–specific deletion of the principal subunit of NMDA receptors substantially reduces this burst firing *in vivo*[7], suggesting that, among other known modulators of DA neuron bursting[8], NMDA receptors are an essential component for the phasic DA response. However, several *in vitro* studies have suggested that NMDA receptor activation alone is not sufficient to switch DA midbrain neurons to a burst-firing mode. A previous study found that the activity of the sodium-potassium ATPase and application of a hyperpolarizing current were necessary for the induction of robust *in vitro* bursting by NMDA[9]. Although the relevant ion channel is unknown for DA neurons, a recent study showed in subthalamic neurons that NMDA receptor stimulation *in vitro* induced the co-activation of K-ATP channels[10]. In pancreatic β-cells, K-ATP channel opening facilitates burst-like firing both *in vitro* and *in vivo*[11,12]. We found that K-ATP channels, which we previously characterized in DA midbrain neurons[3,13,14], gate *in vitro* and *in vivo* bursting selectively in medial SN (m-SN) DA neurons and thereby control novelty-induced exploratory behavior.

K-ATP channels promote neurodegeneration in vulnerable SN DA neurons in chronic mouse models of Parkinson's disease[14]. In addition, L-type calcium channels have been implicated in the differential vulnerability in Parkinson's disease[15]. How these ion channels contribute to the pathophysiology of human SN DA neurons remains unknown. We observed elevated mRNA expression of K-ATP channel and NMDA receptor subunits and a high degree of *in vivo* bursting in human SN DA neurons from Parkinson's disease patients, consistent with the newly described functional role of these potassium channels.

RESULTS

Regional differences of *in vivo* burst firing in DA neurons

The *in vivo* function of K-ATP channels in DA midbrain neurons is unknown. To address this issue, we characterized the spontaneous action potential discharges (unit activity) of individual, juxtacellularly labeled and immunohistochemically identified DA neurons recorded in isoflurane-anesthetized 3-month-old C57bl6N wild-type mice ($n = 46$ neurons, $N = 29$ mice; **Fig. 1** and **Supplementary Table 1**). These tyrosine hydroxylase–expressing neurons were localized in the ventral tegmental area (VTA), m-SN or lateral SN (l-SN). We also tested a subset of these cells ($n = 32$) for the expression of calbindin-D28K, an established

[1]Institute of Neurophysiology, Neuroscience Center, Goethe-University, Frankfurt, Germany. [2]Institute of Applied Physiology, Ulm University, Ulm, Germany. [3]Department of Computer Science and Mathematics, Goethe-University, Frankfurt, Germany. [4]Division of Cellular and Molecular Medicine, Kobe University, Kobe, Japan. [5]Medical Research Council Anatomical Neuropharmacology Unit, Department of Pharmacology and Oxford Parkinson's Disease Centre, Oxford University, Oxford, UK. [6]Surgical Neurology Branch, National Institute of Neurological Disorders and Stroke, US National Institutes of Health, Bethesda, Maryland, USA. [7]These authors jointly directed this work. Correspondence should be addressed to J.R. (roeper@em.uni-frankfurt.de) or B.L. (birgit.liss@uni-ulm.de).

Received 9 March; accepted 16 July; published online 19 August 2012; doi:10.1038/nn.3185

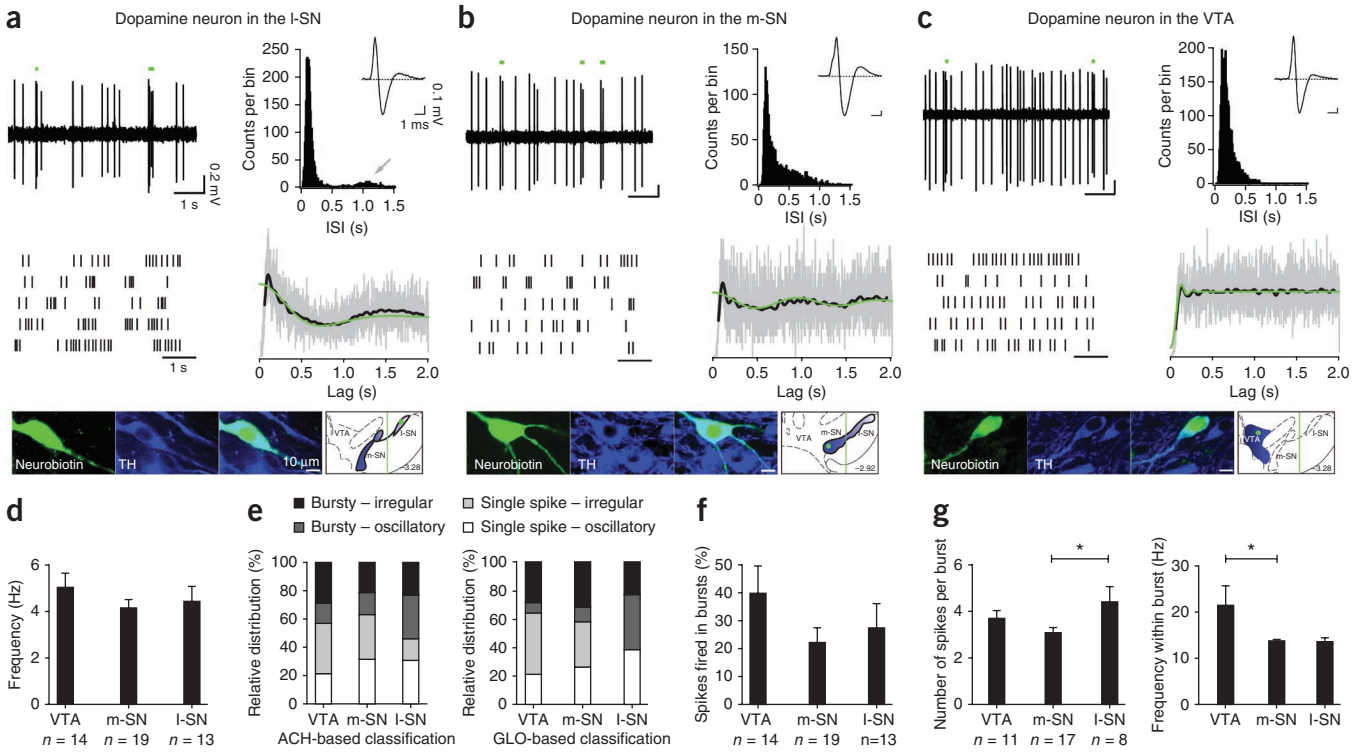

Figure 1 *In vivo* firing characteristics and differences of burst properties of identified DA neurons in the SN and VTA. (**a**) Left, *in vivo* single-unit recording of spontaneous activity of l-SN DA neuron and schematic spike train representation. Burst discharges as defined by 80/160-ms criterion[17] are highlighted by green bars. Top right, corresponding interspike interval (ISI) histogram for >10 min of continuous activity. Inset, extracellularly recorded triphasic action potential[47] (averaged waveform). The bursty-oscillatory pattern was reflected in the bimodal ISI histogram and by the prominent initial peak in the ACH (bottom right; gray lines indicate raw data and the black line represents the smoothed ACH fit; the green line is the GLO model fit; **Supplementary Note**). Bottom row, single-cell labeling, multi-immunofluorescence and confocal microscopy verified the DA phenotype and anatomical position of the recorded neuron in l-SN (dorsal tier, vertical line separates l-SN and m-SN). Shown is a neurobiotin-filled cell (green) expressing tyrosine hydroxylase (TH, blue). (**b**,**c**) *In vivo* single-unit recording of a neurobiotin-filled m-SN DA neuron with a bursty-irregular firing mode (**b**) and of a lateral VTA DA neuron with single spike-irregular mode (**c**). Data are presented as in **a**. (**d**) Mean firing frequencies for identified VTA, m-SN and l-SN DA neurons. (**e**) Relative distributions of four firing patterns (**Supplementary Fig. 1**) defined by ACH- and GLO-based classification. (**f**) Percentage of spikes fired in bursts. (**g**) Distinct region-selective burst properties. Bursts lasted longer in l-SN than m-SN and intraburst frequencies were faster in VTA DA neurons. $*P < 0.05$. For detailed *in vivo* properties and neurochemical subtypes, see **Supplementary Table 1** and **Supplementary Figure 1**. Data are presented as mean ± s.e.m.; *n* is the number of identified neurons (**d**,**f**,**g**).

marker for less vulnerable DA midbrain subpopulations in Parkinson's disease[16] (**Supplementary Fig. 1** and **Supplementary Table 1**).

We examined spontaneous *in vivo* firing of identified DA neurons in the l-SN, m-SN and VTA (**Fig. 1a–c**). DA neurons in these midbrain regions had similar mean discharge rates of 4–5 Hz (**Fig. 1d**) and fired single spikes or bursts in either an oscillatory or irregular manner. To analyze discharge patterns, we used the conventional burst-detection algorithm (percentage of spikes fired in bursts, %SFB, with burst onset of an interspike interval <80 ms (ref. 17) and calculated autocorrelation histograms (ACH)[18]. For quantitative ACH description, we applied our recently established doubly stochastic model (Gaussian locking to a free oscillator, GLO; **Supplementary Fig. 2**)[19]. We found no differences in the incidence of single spike and burst patterns (**Fig. 1e**) across VTA, m-SN and l-SN DA neurons, but detected region-selective differences in the intraburst firing properties (**Fig. 1f**,**g**), suggesting the presence of distinctive burst mechanisms (**Supplementary Table 1**).

K-ATP channels gate burst firing in m-SN DA neurons

In K-ATP channel knockout (*Kir6.2*$^{-/-}$, also known as *Kcnj11*) mice[14], we detected a selective change in the *in vivo* firing properties of m-SN DA neurons. In contrast to m-SN DA neurons recorded in wild-type mice (**Fig. 2a**), they were locked in a regular, single-spike firing pattern (**Fig. 2b**). This pattern shift occurred without changes in mean firing frequencies (**Fig. 2c**). Burst firing, both oscillatory and irregular, was almost completely absent (%SFB m-SN: wild type, 22.3 ± 5.3, $n = 19$ neurons, $N = 13$ mice; *Kir6.2*$^{-/-}$, 6.8 ± 1.5, $n = 21$ neurons, $N = 14$ mice; $P = 0.005$; **Fig. 2d**). The ACH- and GLO-based pattern classification confirmed the selective shift from burst to single-spike firing in m-SN DA neurons (**Fig. 2e**). In contrast, no substantial changes in burst firing were observed in *Kir6.2*$^{-/-}$ DA neurons of l-SN or VTA (**Fig. 2d**,**e**, **Supplementary Fig. 3** and **Supplementary Table 2a**). We examined the regional variation in burst firing of SN DA neurons and found that K-ATP channels were essential only for *in vivo* burst firing of DA neurons in the m-SN (**Fig. 2f**). These m-SN DA neurons mainly project to the dorsomedial striatum (DMS), whereas those of the l-SN project to the dorsolateral striatum, as revealed by tracing of striatal subregions ($n = 10$ injections, data not shown).

To identify those K-ATP channels relevant for m-SN DA bursting, we considered not only postsynaptic K-ATP channels on DA neurons[14], but also K-ATP channels present in nondopaminergic (nonDA) neurons[20]. As K-ATP channel–expressing GABA SN reticulata (SNr) neurons[20] constitute one important component for the synaptic control of *in vivo* burst firing in SN DA neurons[8], we recorded from these cells in anesthetized *Kir6.2*$^{-/-}$ and wild-type mice. Firing rates and

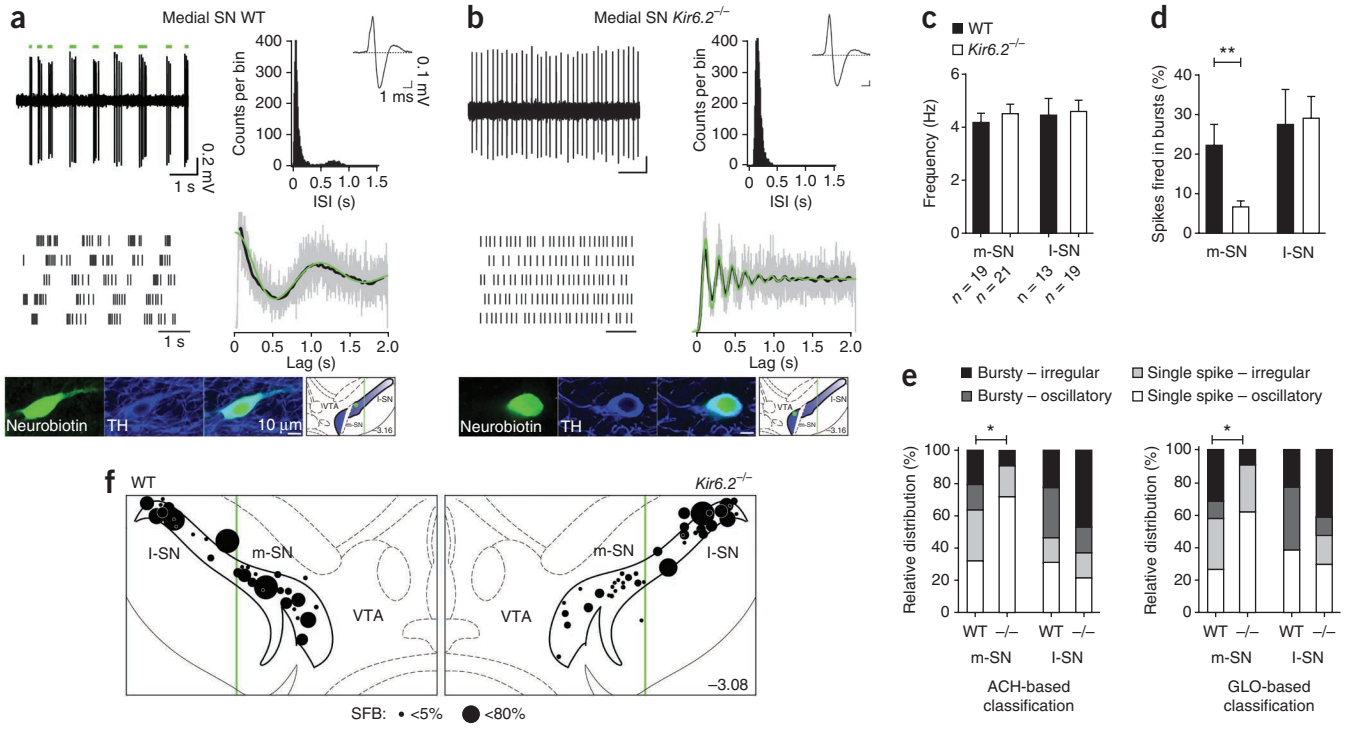

Figure 2 K-ATP channels selectively control *in vivo* burst firing in m-SN DA neurons. (**a**) *In vivo* single-unit activity of m-SN DA neuron recorded in anesthetized wild-type (WT) mice. The bursty-oscillatory pattern was evident in the sample trace, raster plot, biphasic ISI histogram (inset, single action potential) and ACH (with GLO model fit, colors as in **Fig. 1**). Bottom, the recorded neuron was neurochemically identified by neurobiotin filling combined with tyrosine hydroxylase expression. (**b**) *In vivo* single-unit activity of a m-SN DA neuron in a *Kir6.2*$^{-/-}$ mouse displaying single spike-oscillatory firing. Data are presented as in **a**. See **Supplementary Figure 3** for original recordings of l-SN and VTA DA neurons in wild-type and *Kir6.2*$^{-/-}$ mice. (**c**) Mean firing frequencies for m-SN and l-SN DA neurons in wild-type and *Kir6.2*$^{-/-}$ mice (in **c**,**d**, mean ± s.e.m.; *n*, number of identified neurons). (**d**) Spikes that fired in bursts were selectively reduced (3.3-fold) in m-SN DA neurons in *Kir6.2*$^{-/-}$ compared with wild type. $^{**}P < 0.01$. (**e**) The decrease of burst activity in *Kir6.2*$^{-/-}$ m-SN DA neurons was confirmed by changes in ACH- and GLO-based classifications. Pattern distributions differed significantly between m-SN *Kir6.2*$^{-/-}$ and wild type ($^{*}P < 0.05$). See **Supplementary Table 2a** for data and statistics. (**f**) Functional burst map. Wild-type (left) and *Kir6.2*$^{-/-}$ (right) DA neurons were plotted according to their position in the SN (bregma, –3.08 mm)[48]. Symbol size scales with %SFB. Note the clustering of non-bursting m-SN DA neurons in *Kir6.2*$^{-/-}$ compared with wild type.

patterns of electrophysiologically identified SNr neurons were not affected by the lack of K-ATP channels (**Supplementary Table 2b**). Juxtacellular labeling of a subset of these SNr neurons confirmed their nonDA phenotype ($n = 8$ of 28 neurons, $N = 13$ mice, data not shown). We next addressed the issue of whether postsynaptic K-ATP channels in m-SN DA neurons are necessary for bursting *in vitro* and *in vivo*.

We tested whether pharmacological activation of K-ATP channels was sufficient to induce *in vitro* bursting in synaptically isolated m-SN DA neurons in the presence of NMDA. We used cell-attached recordings to maintain the metabolic integrity and avoid nonphysiological K-ATP channel activation. Pharmacological activation of K-ATP channels alone by the SUR1-selective agonist NN414 (10 µM)[21] reduced the rate of spontaneous firing of SN DA neurons in brain slices (**Supplementary Fig. 4b**). However, in the presence of 30 µM NMDA (**Fig. 3a**), NN414-mediated K-ATP activation was sufficient to trigger burst-like discharges in m-SN DA neurons in wild-type mice. In contrast, 30 µM NMDA + NN414 failed to induce bursting in m-SN DA neurons in *Kir6.2*$^{-/-}$ mice (**Fig. 3b–e**). Furthermore, we found that, in the presence of 30 µM NMDA, bursting was acutely switched on by co-application of 10 µM NN414 (~sevenfold increase of %SFB; **Supplementary Fig. 4a**) and was subsequently almost completely switched off by application of 300 µM tolbutamide, a K-ATP channel inhibitor (**Supplementary Fig. 4a**). These findings indicate that K-ATP channel activity is essential for NMDA-mediated *in vitro* bursting in m-SN DA neurons. Moreover, NN414-mediated K-ATP channel activation was sufficient to enhance the maximal firing rates of m-SN DA neurons induced by somatic current injection (**Fig. 4a**). In contrast, maximal firing rates in *Kir6.2*$^{-/-}$ or in wild-type mice in the presence of 300 µM tolbutamide remained below the *in vivo* intraburst frequencies (**Fig. 4b–d**). These data suggest that the functional consequences of K-ATP channel activation are context dependent, either slowing down spontaneous discharge or, in the presence of NMDA, increasing bursting.

Selective silencing of K-ATP channels in SN DA neurons

We next asked whether K-ATP channel activity in m-SN DA neurons is also necessary for their spontaneous bursting *in vivo*. We established a strategy for virally mediated (recombinant adeno-associated virus, serotype 2; rAAV2) cell-selective expression of dominant-negative or wild-type Kir6.2 subunits (Kir6.2_DN and Kir6.2_WT, respectively) and enhanced GFP (eGFP) controls in SN DA neurons in adult wild-type mice. First, we determined the rAAV2 titer and volume that, when infused into the midbrain, led to a cell type–selective transduction of DA neurons (89%, 408 of 459 transduced cells expressed tyrosine hydroxylase and hemagglutinin (HA), $N = 3$ mice) in a SN-selective manner (**Fig. 5a–d** and **Supplementary Fig. 5a**). *In vivo* electrophysiology revealed that eGFP expression alone induced significant changes ($P = 0.038$) in burst firing, which precluded its use as a control (**Supplementary Fig. 5b**). We therefore used an HA-tag added to Kir6.2_DN or Kir6.2_WT constructs for expression control.

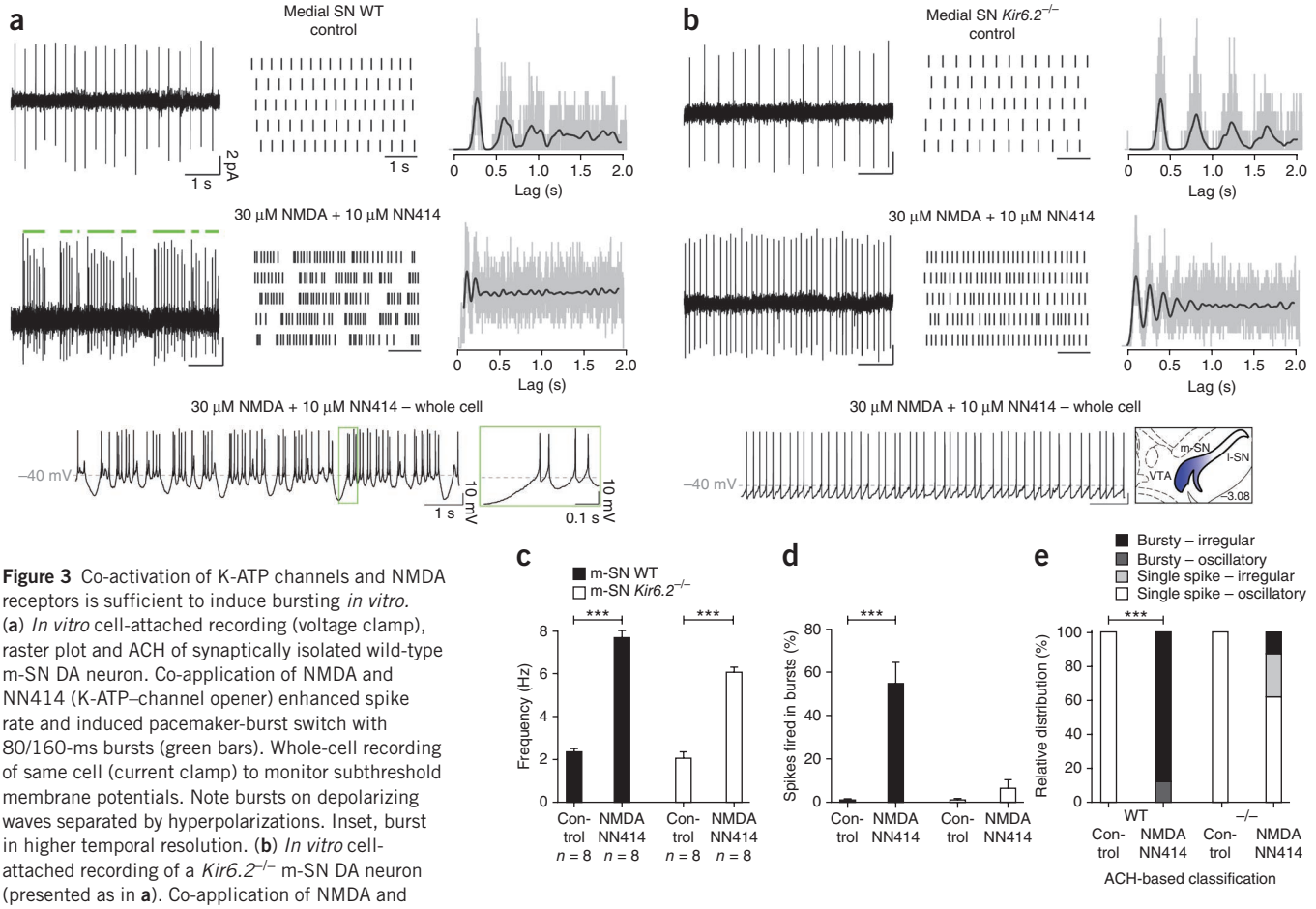

Figure 3 Co-activation of K-ATP channels and NMDA receptors is sufficient to induce bursting *in vitro*. (**a**) *In vitro* cell-attached recording (voltage clamp), raster plot and ACH of synaptically isolated wild-type m-SN DA neuron. Co-application of NMDA and NN414 (K-ATP–channel opener) enhanced spike rate and induced pacemaker-burst switch with 80/160-ms bursts (green bars). Whole-cell recording of same cell (current clamp) to monitor subthreshold membrane potentials. Note bursts on depolarizing waves separated by hyperpolarizations. Inset, burst in higher temporal resolution. (**b**) *In vitro* cell-attached recording of a *Kir6.2*$^{-/-}$ m-SN DA neuron (presented as in **a**). Co-application of NMDA and NN414 increased firing rate but not bursting. Note continuous single-spike oscillatory firing, in both on-cell and whole-cell recording of same cell. Brain atlas shows rostromedial SN (blue), where all *in vitro* recordings were performed. (**c**) Mean firing frequencies for m-SN DA neurons in wild type and *Kir6.2*$^{-/-}$. NMDA and NN414 significantly enhanced *in vitro* frequencies (wild type, 2.4 ± 0.2 and 7.7 ± 0.3 Hz, $P < 0.0001$, $t = 17.83$, $n = 8$ recorded cells, $N = 8$ animals; *Kir6.2*$^{-/-}$, 2.1 ± 0.3 and 6.1 ± 0.2 Hz, $P < 0.0001$, $t = 8.72$; in **c**,**d**, $n = 8$, $N = 8$; paired *t* tests, mean ± s.e.m.). ***$P < 0.001$. (**d**) %SFB was significantly increased after NMDA + NN414 in wild type (1.1 ± 0.4 and 54.5 ± 9.9%, $P = 0.001$, $t = 5.29$), but not in *Kir6.2*$^{-/-}$ (1.1 ± 0.6 and 6.4 ± 3.9%, $P = 0.24$, $t = 1.29$) m-SN DA cells. See **Supplementary Figure 4a** for reversible pharmacological induction of K-ATP–gated bursting. (**e**) K-ATP and NMDA receptor co-activation–mediated bursting in wild-type m-SN DA neurons was confirmed by respective changes in ACH-based classifications. Pattern distributions differed significantly for wild type ($P < 0.001$, $\chi^2 = 16$), but not *Kir6.2*$^{-/-}$ ($P = 0.2$, $\chi^2 = 3.69$; Pearson's Chi-squared test).

To rule out potential confounds, we carefully tested for the expression of virally coded proteins by neurons in ten brain areas that give rise to afferent projections to SN DA cells (**Supplementary Fig. 6a**). We also tested for the presence of viral proteins in axon terminals in close apposition to m-SN DA neurons (**Supplementary Fig. 6b**). We found no evidence for the presence of HA-tagged Kir6.2_DN in nine of ten input areas, with the exception of the SNr, in which just a few tyrosine hydroxylase–negative, HA-positive cells were observed (n = ~30 SNr nonDA HA-positive neurons per mouse, $N = 2$ mice; n = ~4,100 SNc DA HA-positive neurons per mouse, $N = 3$ mice). In addition, less than 1.5% of all of the GABAergic and glutamatergic axon terminals apposed to m-SN DA neurons expressed HA (**Supplementary Fig. 6b**). Thus, Kir6.2_DN transgene expression by nonDA neurons was limited to the SNc, which accounted for about 9% of transduced cells. We carried out standard *in vitro* whole-cell and on-cell recordings of these fast-firing nonDA SNc neurons (10–15 Hz) to probe for functional K-ATP channels. These neurons showed no K-ATP washout currents or rate changes in response to the SUR1-selective K-ATP channel opener NN414 (**Supplementary Fig. 4b**), indicating the absence of K-ATP channels in these putative GABAergic neurons[13]. Our control experiments strongly argue against any substantial contributions from extrinsic afferents or local network inputs after viral delivery of dominant-negative Kir6.2 subunits.

We then studied functional K-ATP channels in SN DA neurons, transduced with either HA-tagged Kir6.2_WT or Kir6.2_DN subunits, using whole-cell patch-clamp recordings in brain slices. Maximal K-ATP channel activation was achieved by dialysis with ATP-free pipette solutions. As previously described, no K-ATP washout currents were observed in SN DA neurons in *Kir6.2*$^{-/-}$ mice[14]. Expression of Kir6.2_DN also led to a complete silencing of K-ATP channels in SN DA neurons 2 weeks after *in vivo* transduction. In contrast, transduction with Kir6.2_WT did not affect the maximal washout currents (**Fig. 5e**), consistent with Kir6.2 subunits having an endoplasmic reticulum retention motif[22].

We then combined rAAV2-based K-ATP channel silencing with recording and juxtacellular labeling of individual DA neurons in anesthetized mice to define the electrophysiological phenotype of identified, virally transduced DA neurons *in vivo* ($n = 30$ neurons, $N = 18$ mice). Expression of the dominant-negative Kir6.2 subunits, but not of wild-type Kir6.2 subunits, reduced burst firing in m-SN DA neurons (%SFB: Kir6.2_WT, 22.1 ± 4.0, $n = 9$ identified neurons; Kir6.2_DN, 9.1 ± 3.8, $n = 8$; $P = 0.033$, unpaired *t* test; **Fig. 6** and **Supplementary Table 3**)

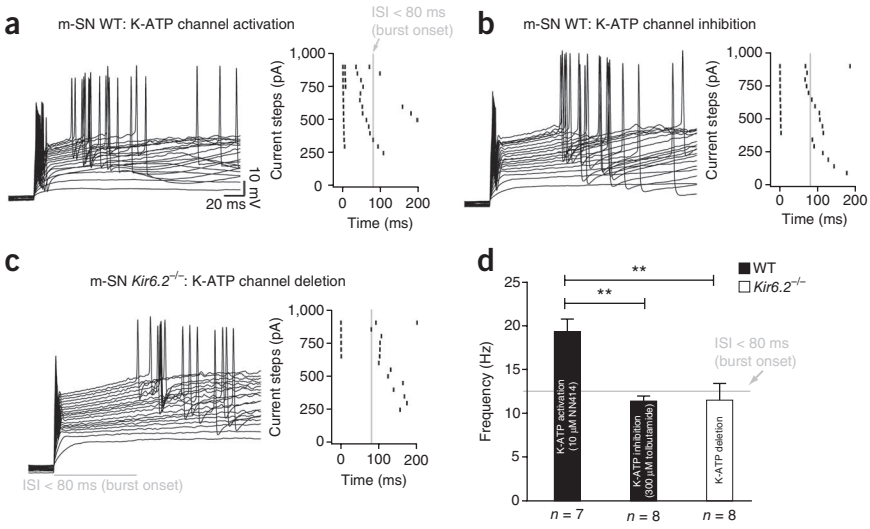

Figure 4 K-ATP channel activation shifts maximal firing frequencies induced by current injection into the burst range in m-SN DA neurons *in vitro*. (**a**) *In vitro* whole-cell patch-clamp recording (current clamp) of a m-SN DA wild-type neuron showing spike discharges in response to consecutive depolarizing current steps from –70 mV (increments of 50 pA, 2-s current pulse, 225 ms shown with time relative to stimulus onset). K-ATP channels were activated by the selective SUR1–K-ATP–channel opener NN414 (10 µM). Right, post initial-spike time histogram. Current steps of increasing amplitude triggered high-frequency, burst-like discharges. The gray line at 80 ms after the initial spike indicates the threshold for burst onset as defined *in vivo*[17]. Note the high spike probability in this period. (**b**,**c**) Current-clamp recordings (presented as in **a**) of a wild-type m-SN DA neuron in the presence of 300 µM tolbutamide (**b**) and of a *Kir6.2*$^{-/-}$ m-SN DA neuron (**c**). Note the prolonged intervals in the absence of K-ATP channels. (**d**) Activation of K-ATP channels *in vitro* induced fast frequencies between the initial and the first somatodendritic spike. K-ATP–triggered burst-like discharges (19.3 ± 1.5 Hz, $n = 7$, $N = 5$) were clearly faster than the *in vivo* burst threshold (gray line at 12.5 Hz). In contrast, pharmacological or genetic inactivation of K-ATP channels using tolbutamide or *Kir6.2*$^{-/-}$ mice resulted in significantly slower discharge rates (11.4 ± 0.6 Hz, $n = 8$, $N = 4$; 11.6 ± 1.9 Hz, $n = 8$, $N = 2$; respectively; $P = 0.001$, $F = 9.87$, one-way ANOVA with Bonferroni post-tests). $^{**}P < 0.01$. Data are presented as mean ± s.e.m., *n*, number of recorded neurons; *N*, number of mice.

to a degree similar to that seen for these neurons recorded in *Kir6.2*$^{-/-}$ mice. Consequently, m-SN DA neurons expressing Kir6.2_DN, but not those expressing Kir6.2_WT, tended to be locked in a regular single-spike firing mode, which was confirmed by ACH- and GLO-based classification (**Fig. 6c**). Moreover, the action potential waveforms of m-SN DA neurons expressing Kir6.2_DN showed a delayed repolarization phase as compared with that of neurons expressing Kir6.2_WT (**Fig. 6d**). These changes in firing pattern and action potential repolarization were not found in identified l-SN DA neurons expressing Kir6.2_DN (data not shown), suggesting a selective *in vivo* effect of virally mediated K-ATP channel silencing on m-SN DA neurons.

K-ATP channels enable novelty-dependent behavior

The degree of *in vivo* baseline bursting of DA neurons under isoflurane anesthesia that we observed is similar to that seen in awake rodents and primates[23,24]. We therefore reasoned that K-ATP channel–gated

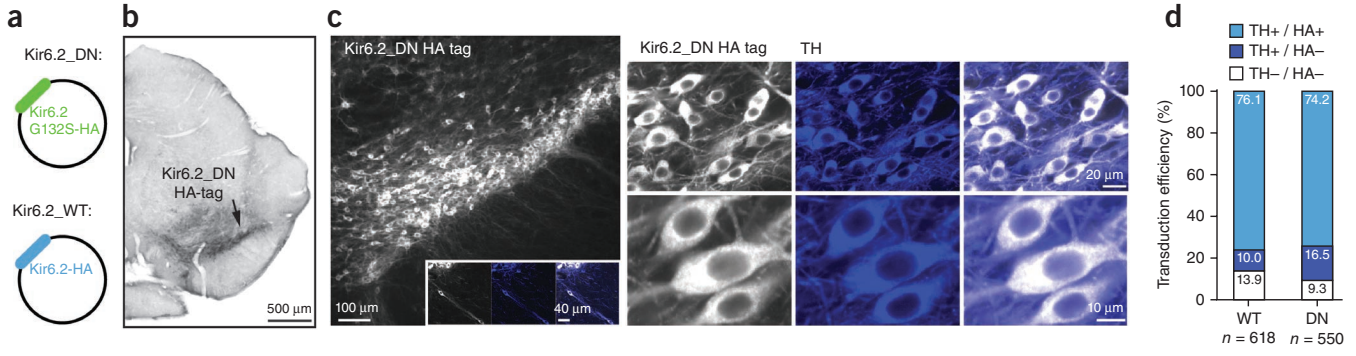

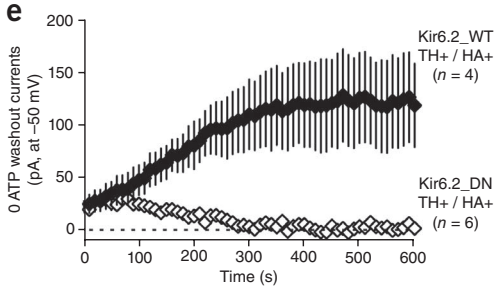

Figure 5 Virus-mediated expression of dominant-negative Kir6.2 pore mutant induced selective functional silencing of K-ATP channels in SN DA neurons. (**a**) rAAV2-coded HA-tagged dominant-negative (Kir6.2G132S-HA or Kir6.2_DN) and wild-type Kir6.2 subunits (Kir6.2_WT, for control) were used. (**b**,**c**) DAB (**b**) and fluorescent labeling (**c**) immunocytochemistry revealed selective and efficient expression of HA-tagged Kir6.2_DN subunits (white) across the entire m-SN and l-SN and in somatodendritic domains of single DA neurons (that is, tyrosine hydroxylase positive, blue). Inset in **c** highlights a selectively transduced tyrosine hydroxylase–positive neuron in the SNr. Right, confocal images showing an overlay of HA and tyrosine hydroxylase signals at a higher magnification. (**d**) Quantification of transduction efficiency (tyrosine hydroxylase and HA double-positive neurons) across the entire SN (Kir6.2_WT and Kir6.2_DN; *n*, total number of SN neurons counted, $N = 6$ mice). Nigral tyrosine hydroxylase–positive neurons expressed mutant and wild-type Kir6.2-HA constructs to a similar degree. In contrast, only a minor fraction of VTA DA neurons was transduced (Kir6.2_DN, 32.9% TH^+ HA^+, 57.6% TH^+ HA^-, 9.5% TH^- HA^+, $n = 575$; Kir6.2_WT, 34.9%, 38%, 27.1%; $n = 939$, $N = 6$ mice; data not shown and **Supplementary Figs. 5** and **6**). (**e**) Suppression of K-ATP–mediated currents by Kir6.2_DN. K-ATP washout currents were absent *in vitro* during whole-cell patch-clamp recordings of Kir6.2_DN-transduced SN DA cells. Kir6.2_WT expression did not affect K-ATP channel activation (steady-state washout currents: Kir6.2_DN, 0.5 ± 6.3 pA, $n = 6$ recorded neurons; Kir6.2_WT, 118.7 ± 39.7 pA, $n = 4$; $P = 0.014$ (U = 0.0), Mann-Whitney U test; mean ± s.e.m., $N = 8$ mice). Tyrosine hydroxylase and HA co-expression was confirmed by neurobiotin-filling and confocal analyses (data not shown).

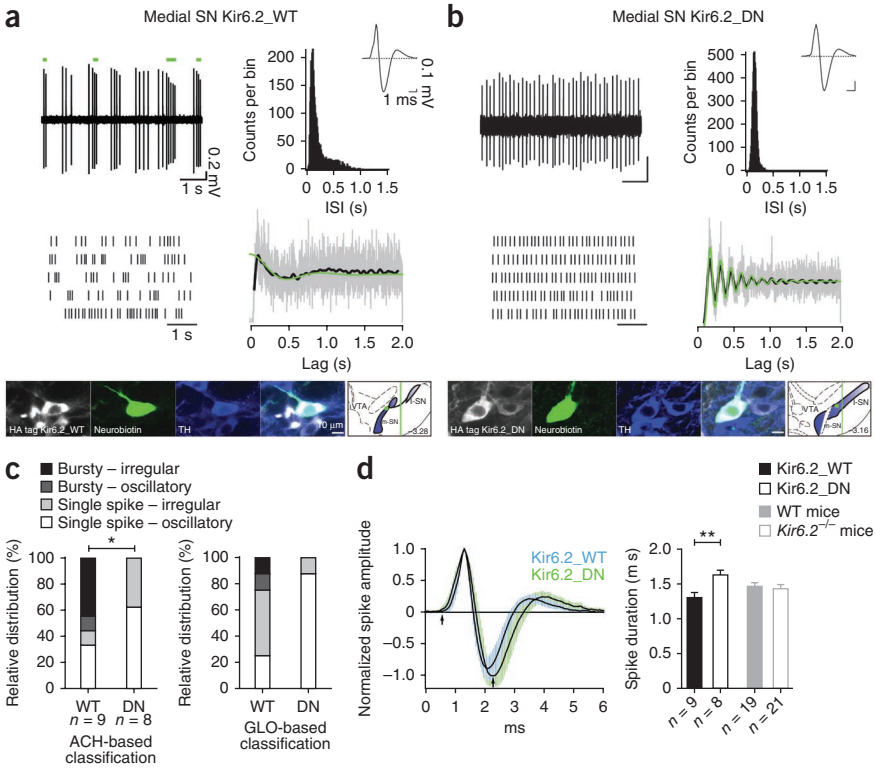

Figure 6 Cell-selective silencing of K-ATP channels in SN DA neurons using virally mediated gene transfer is sufficient to prevent burst firing in m-SN neurons. (**a**) *In vivo* single-unit activity of a m-SN DA neuron transduced with rAAV2 constructs expressing wild-type Kir6.2 subunits (Kir6.2_WT). Similar to m-SN DA wild-type cells (**Figs. 1b** and **2a**), it fired in a bursty pattern as shown in raw trace, raster plot, ISI histogram (inset, single action potential) and ACH with GLO-model fit. Neurobiotin-labeling (green) of the recorded neuron identified transduction with HA-tagged Kir6.2_WT constructs (white) and coexpression of tyrosine hydroxylase (blue). (**b**) Selective silencing of postsynaptic K-ATP channels by expression of Kir6.2_DN in m-SN DA neurons prevented burst firing. Data are presented as in **a**. The neurobiotin-filled neuron coexpressed HA-tagged Kir6.2_DN and tyrosine hydroxylase and was located in the m-SN. Although mean firing frequencies were similar, the percentage of spikes fired in bursts was significantly reduced (2.4-fold, $P = 0.033$) in Kir6.2_DN compared with Kir6.2_WT (see **Supplementary Table 3**). (**c**) Decrease of burst activity in Kir6.2_DN m-SN DA neurons compared with Kir6.2_WT. ACH- and GLO-based pattern classification differed significantly between dominant negative and wild type (ACH, $P = 0.041$; GLO, $P = 0.053$). Data are presented as mean ± s.e.m. (*n*, number of identified neurons, see **Supplementary Table 3**). $^*P < 0.05$. (**d**) Overlaid plot of mean average spike shapes of m-SN neurons expressing Kir6.2_WT (blue, s.e.m.) and Kir6.2_DN (green, s.e.m.). Note the prolonged action potential duration in Kir6.2_DN compared with Kir6.2_WT. For comparison, spike durations from wild-type and *Kir6.2*$^{-/-}$ mice are plotted (gray; $P = 0.016$, $F = 2.6$, one-way ANOVA with Bonferroni post test, $^{**}P < 0.01$).

burst firing in m-SN DA neurons might be functionally relevant in awake, freely moving mice. To explore the behavioral consequences of SN DA neuron subtype-selective K-ATP channel silencing, we tested spontaneous open field behavior of mice with bilateral K-ATP channel silencing across the whole SN (medial and lateral) or in only the l-SN. For reference, we also studied wild-type and *Kir6.2*$^{-/-}$ mice.

We identified a selective reduction of initial locomotor activation in *Kir6.2*$^{-/-}$ mice compared with wild-type controls in a novel open field (open field day 1; **Fig. 7a**). This difference in initial locomotion was not observed in consecutive open field sessions (data not shown), indicating a novelty-selective phenotype, which is consistent with our previous behavioral characterization of *Kir6.2*$^{-/-}$ mice[25]. In addition, rearing frequencies were significantly smaller ($P < 0.0001$) in *Kir6.2*$^{-/-}$ mice than in wild-type mice throughout the entire testing period (**Fig. 7b**). These results, which were twice replicated in additional *Kir6.2*$^{-/-}$ and wild-type mouse cohorts (data not shown), indicate a novelty-dependent deficit in initiation of exploratory behavior in global K-ATP knockout mice. Virally mediated silencing of K-ATP channels in DA neurons across the whole SN (Kir6.2_DN m+l-SN) phenocopied the selective deficit in novelty-induced locomotor activation and reduction in rearing frequencies (**Fig. 7c–e**). In contrast, silencing of K-ATP channels only in neurons of the l-SN had no significant effects on locomotion ($P = 0.92$, $t = 0.1$, $F = 2.04$) and rearing ($P = 0.61$, $t = 0.51$, $F = 1.09$; unpaired *t* tests) compared with wild-type mice. We found no changes in center avoidance between Kir6.2_DN l-SN– and m+l-SN–injected mice, suggesting that K-ATP channels in SN DA neurons were not involved in anxiety-mediated behavioral inhibition (data not shown).

These results indicate that K-ATP channel signaling in m-SN, but not l-SN, DA neurons is necessary for wild-type–like exploratory behavior. Taken together, these *in vivo* and *in vitro* findings suggest that K-ATP channel-gated bursting in m-SN DA neurons is crucial for context-dependent exploratory behavior.

K-ATP channels and Parkinson's disease

The burst-promoting *in vivo* function of active K-ATP channels in SN DA neurons might also be relevant in Parkinson's disease. Thus, we first studied the expression of K-ATP channel subunits in human SN DA neurons in post mortem tissue from Parkinson's disease patients and control subjects. We used our established ultraviolet laser-microdissection (UV-LMD) and quantitative mRNA expression profiling techniques for remaining DA neurons[26], which are mainly found in the medial aspects of the SN (identified by the presence of neuromelanin; **Fig. 8a**).

We examined the mRNA expression of the K-ATP channel subunits Kir6.2, SUR1 and SUR2. We also profiled the expression of the calcium-binding protein calbindin and the NMDA receptor subunit NR1, which are both involved in SN DA neuron burst activity (**Fig. 3** and **Supplementary Fig. 1**) and have been implicated in Parkinson's disease pathophysiology. We found a significant increase of calbindin expression (approximately sixfold, $P < 0.001$) and a significant increase of NR1 expression (approximately tenfold, $P < 0.001$) in surviving SN DA neurons from Parkinson's disease brains compared with neurons from controls. In addition, we detected significantly higher mRNA levels (approximately twofold, $P < 0.05$) of the regulatory K-ATP channel subunit SUR1 in SN DA neurons from Parkinson's disease patients compared with neurons from controls. In contrast, mRNA expression of SUR2 and the pore-forming subunit Kir6.2 were not altered (**Fig. 8b** and **Supplementary Table 4a**). These results suggest that the K-ATP channel subunit SUR1 is selectively transcriptionally upregulated in human SN DA neurons in Parkinson's disease, which might be consistent with increased burst firing. To directly assess this possibility,

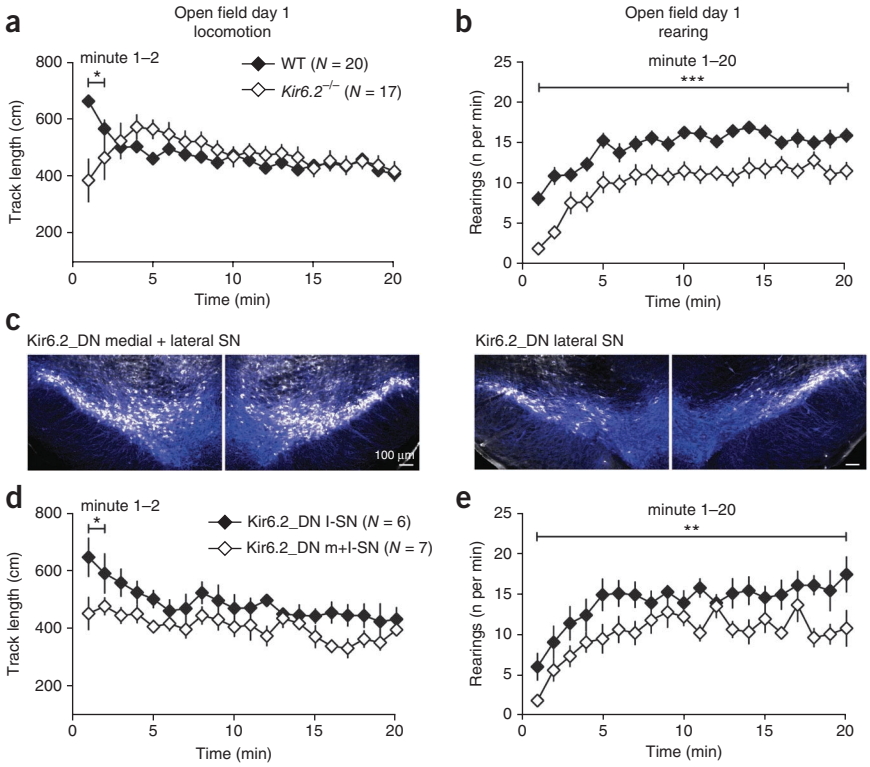

Figure 7 K-ATP channels in m-SN DA neurons are necessary for novelty-dependent exploratory behavior. (**a**) Locomotion in novel open field (track length per min). Note the decreased locomotion (minutes 1–2) in *Kir6.2*$^{-/-}$ (856 ± 141 cm, $N = 17$ mice) compared with the increased locomotion in wild type (1,230 ± 45 cm, $N = 20$, $P = 0.011$, $t = 2.69$, $F = 8.26$). In contrast, no significant difference in cumulative locomotion was observed in minutes 3–20 ($P = 0.27$, $t = 1.12$, $F = 7.4$). All data given as mean ± s.e.m. and analyzed with unpaired *t* tests. $^{*}P < 0.05$. (**b**) Rearings in the novel open field (*n* per minute). The numbers of rearings were significantly smaller in *Kir6.2*$^{-/-}$ (201 ± 15) than in wild type (290 ± 9, $P < 0.0001$, $t = 5.16$, $F = 2.42$). $^{***}P < 0.001$. (**c**) Immunohistochemical confirmation of SN-selective bilateral transduction of DA neurons in mice for open field testing (13–14 d after injection). HA-tagged Kir6.2_DN viral constructs (white) were expressed in most SN tyrosine hydroxylase–positive cells (blue). Expression was either targeted at the entire SN (m+l-SN, left) or restricted to l-SN (control, right). (**d**) Locomotion in novel open field using mice with bilateral K-ATP channel silencing across the whole SN or in just the l-SN. Note the absence of initially increased locomotion in Kir6.2_DN m+l-SN mice (minute 1–2, 934 ± 70 cm, $N = 7$ virus-injected mice) compared with l-SN controls (1,240 ± 118 cm, $N = 6$, $P = 0.042$, $t = 2.3$, $F = 2.44$). Significant difference in cumulative locomotion was also observed for minute 3–20 ($P = 0.046$, $t = 2.26$, $F = 1.5$). (**e**) Rearings in novel open field of mice where the entire or only l-SN was transduced with Kir6.2_DN. The numbers of rearings were significantly smaller in Kir6.2_DN m+l-SN (minute 1–20, 201 ± 12, $N = 7$) than in l-SN (280 ± 17, $N = 6$, $P = 0.0028$, $t = 3.83$, $F = 1.76$). $^{**}P < 0.01$.

we analyzed firing rates and patterns of viable human SN DA neurons *in vivo*, intra-operatively recorded from Parkinson's disease patients[27]. In the absence of genuine control data from healthy human subjects, electrophysiological recordings of identified SN DA neurons in anesthetized rodents and of putative DA neurons in awake nonhuman primates must suffice for a comparative analysis. Compared with our recordings from mice, awake rodents[24] and monkeys[23], human SN DA neurons from Parkinson's disease patients ($n = 13$ cells, $N = 10$ subjects) showed no difference in mean rates, but displayed twofold higher burst firing (**Fig. 8c–e** and **Supplementary Table 4c**). The ACH- and GLO-pattern analyses confirmed the dominance of burst activity in surviving SN DA neurons recorded in Parkinson's disease patients (**Fig. 8f**). In summary and in the context of our mouse experiments, our single-cell molecular and electrophysiological data from humans suggest that increased K-ATP channel–gated burst firing might contribute to the phenotype of surviving SN DA neurons in Parkinson's disease.

DISCUSSION

K-ATP channels in m-SN DA neurons gate burst firing

K-ATP channels are widely expressed in excitable tissues, where, in most cases, they act as metabolically controlled excitation brakes by matching excitability to cellular energy states[28]. In contrast with this conventional role, we found that K-ATP channels in m-SN DA neurons *in vivo* act as cell type–selective gates for excitatory burst firing. This burst-promoting role of K-ATP channels is not unprecedented, as their opening facilitates burst-like discharges in pancreatic β-cells[11,12]. Thus, K-ATP channels complement established mechanisms in burst control for DA neurons. Recent studies employing DA-selective knockout mice confirmed that NMDA receptors are important for bursting[7,29]. Consistent with previous *in vitro* studies[30,31], NMDA receptor stimulation also led to robust bursting in m-SN DA neurons, but only when K-ATP channels were co-activated. In addition to NMDA receptors, molecular and pharmacological studies have suggested that GABAergic disinhibition is important for gating of *in vivo* bursting and phasic signaling in DA neurons[8,32]. Furthermore, bursting is also facilitated by nicotinic acetylcholine receptors[33], mGluRs[34] and inhibition of SK channels in DA neurons[35]. Notably, our carefully controlled cell-selective silencing of K-ATP channels in SN DA neurons revealed no evidence that pre- or postsynaptic K-ATP channels contribute to bursting in any of the main afferent projection areas, axon terminals or in local nonDA neurons.

Although pharmacological co-activation of NMDA receptors and K-ATP channels induced robust bursting *in vitro* in m-SN DA neurons, indicating that their interaction *in vivo* might also be sufficient to generate bursting, an important difference remains. Under *in vitro* conditions, K-ATP channels in intact DA neurons were not sufficiently activated to induce the switch to bursting in the presence of NMDA. This implies that K-ATP channels *in vivo* possess a higher open probability as a result of yet unidentified metabolic or other upstream mechanisms. There are various metabolic signals operative *in vivo* in the DA midbrain system, such as leptin[36] or ghrelin[37], that might enhance K-ATP channel gating in m-SN DA neurons sufficiently to be engaged in bursting and thereby influence dopamine-dependent behavior. However, the detailed analysis of synaptic and metabolic mechanisms that control K-ATP channel–gated bursting in SN DA neurons will need to be addressed in future studies.

K-ATP channels control novelty-induced exploration

Our data indicate that K-ATP channel–gated bursting occurs selectively in m-SN DA neurons that project to the DMS, where tonic and

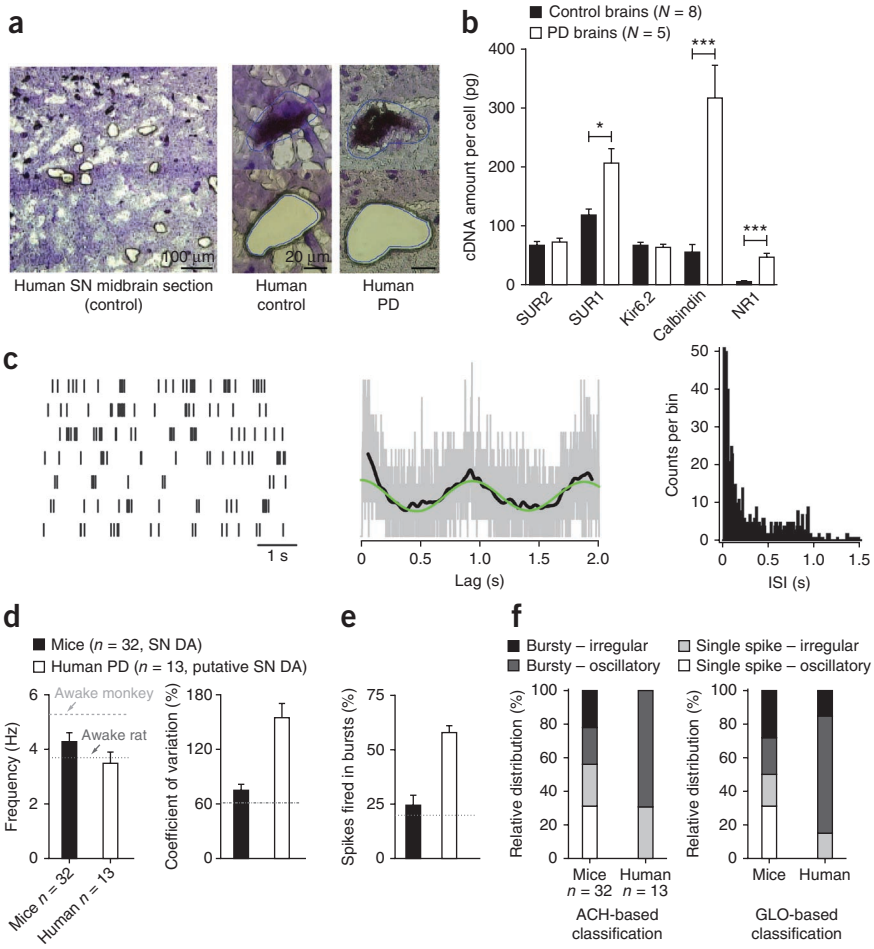

Figure 8 Increased mRNA levels of the K-ATP channel subunit SUR1 and high burst firing in SN DA neurons from Parkinson's disease patients. (**a**) Neuromelanin-positive SN neurons isolated via laser microdissection from cresyl violet–stained cryosections of human post mortem midbrain tissue (left). Individual neurons in control (middle) and Parkinson's disease brain tissue (PD, right) before and after UV-LMD. (**b**) Selective transcriptional dysregulation of the K-ATP channel subunit SUR1 in SN DA neurons from human Parkinson's disease midbrains. Cell-specific average mRNA levels of SUR1, calbindin and NR1 were significantly increased in Parkinson's disease compared with control. mRNA levels of Kir6.2 or SUR2 were not different. $*P < 0.05$, $***P < 0.001$. Data are presented as mean ± s.e.m. (N = number of brains, see **Supplementary Table 4a**). (**c**) Firing activity of a putative SN DA neuron recorded in a Parkinson's disease patient presented as raster plot, ACH and ISI histogram. (**d**) Mean frequency and coefficient of variation of putative DA neurons recorded from Parkinson's disease patients are plotted in comparison to SN DA neurons (n = 32, **Fig. 1**), awake rats[24] (dark gray, dashed line) and awake monkeys[23] (gray, dashed line). Mean frequencies were similar, but there was higher irregularity in neurons from Parkinson's disease patients. Bars represent mean ± s.e.m. (n, number of single units). (**e**) High burst firing in human SN DA neurons of Parkinson's disease patients. %SFB was 2.4-fold higher in Parkinson's disease patients compared to rodents. (**f**) Dominance of bursty-oscillatory firing pattern in human Parkinson's disease SN DA neurons revealed by ACH- and GLO-based classification (see **Supplementary Table 4b**).

phasic DA release controls a corticostriatal circuit involved in cognitive functions and goal-directed behavioral activation[1,2,38]. Recent evidence identified burst firing of DA neurons as creating a striatal dopamine receptor 1–dependent Go signal for locomotor activation and self-paced action sequences[6,39]. Accordingly, we found that cell-selective K-ATP channel function in m-SN DA neurons was necessary for the initiation of novelty-dependent exploratory behavior. Selective depletion experiments in the DMS revealed that DA release in this striatal region is important for responding to contextual changes in goal-directed behavioral strategies[40]. This is consistent with the strong input to DMS from the entorhinal cortex[41], which reads out a hippocampal spatial novelty signal[42].

Human imaging studies have also shown that novelty leads to a strong activation of the VTA and SN region[43], particularly in the rostromedial part, which selectively responds to novel, but not reward-predicting, stimuli[5]. The rostromedial localization of the novelty-selective region in the human midbrain is consistent with our findings that m-SN DA neurons are important for novelty-induced exploration in the mouse. In conclusion, our data are consistent with a selective behavioral function of K-ATP channel–gated bursting in m-SN DA neurons as an essential trigger for DA-dependent initiation of exploratory behavior, either in response to contextual changes or as a constant bias in explore-exploit conflicts.

K-ATP channels and Parkinson's disease

Our expression data and functional recordings from human SN DA neurons revealed elevated expression of K-ATP channel and NMDA receptor subunits in Parkinson's disease as well as high burst firing. These findings are consistent with an increased number of functional K-ATP channels that, in concert with concomitantly enhanced NMDA receptor function, facilitate burst firing and might reflect a compensatory upregulation to maintain striatal DA levels. Alternatively, m-SN DA neurons might already be disturbed during an early stage of Parkinson's disease, consistent with results documenting reduced novelty seeking, reduced exploratory excitability and choice perseveration in Parkinson's disease patients[44,45].

In addition, enhanced K-ATP channel–dependent bursting in DA neurons in Parkinson's disease might also have implications for the neurodegenerative process itself. K-ATP channel–gated *in vivo* burst firing in already metabolically challenged SN DA neurons could promote excitotoxicity and increased calcium loading synergistically with NMDA receptors and L-type Ca^{2+} channels[15], whereas defects in *PARK* genes and environmental factors further reduce mitochondrial calcium buffering capacities and accelerate calcium-triggered reactive oxygen species production[46]. Mitochondria-generated reactive oxygen species in turn activate K-ATP channels in highly vulnerable SN DA neurons[14] and could lead to a vicious spiral of metabolically amplified, burst-triggered excitotoxicity and calcium overload. This positive feedback might lock SN DA neurons in a highly stressful bursting state *in vivo*, potentially accelerating their degeneration. Consequently, our data might suggest that stabilizing an *in vivo* single-spike mode by K-ATP channel modulation results in neuroprotection for SN DA neurons.

METHODS

Methods and any associated references are available in the online version of the paper.

Note: Supplementary information is available in the online version of the paper.

ACKNOWLEDGMENTS

We thank S. Petzoldt, H. Schalk and A. Parg for assistance in immunohistochemistry, and M. Fauler for mRNA expression data analysis. The study was supported by Gemeinnützige Hertiestiftung (J.R. and B.L.), SFB815 (J.R.), SFB497 (B.L.), BMBF Nationales Genomforschungsnetzwerk NGFN-II/plus (01GS08134, J.R. and B.L.), Alfried Krupp prize (B.L.), LOEWE-Schwerpunkt Neuronale Koordination Forschungsschwerpunkt Frankfurt NeFF (J.R. and G.S.), Bernstein Fokus Neurotechnology Frankfurt (G.S. and M.B.), doctoral fellowship Studienstiftung des deutschen Volkes (J.S.) and Medical Research Council UK (U138197109, P.J.M.).

AUTHOR CONTRIBUTIONS

J.S. carried out *in vivo* electrophysiology, juxtacellular labeling (training by P.J.M.), viral gene transfer, retrograde tracing, immunocytochemistry, microscopy and data analyses. V.K. and J.S. carried out animal behavior experiments. J.R. performed *in vitro* electrophysiology. The GLO model was designed by M.B. and G.S. F.S. and B.L. carried out laser microdissection and molecular biology. S.S. generated *Kir6.2*$^{-/-}$. K.A.Z. performed human SN recordings. J.S., P.J.M., B.L. and J.R. designed the study and wrote the manuscript.

COMPETING FINANCIAL INTERESTS

The authors declare no competing financial interests.

Published online at http://www.nature.com/doifinder/10.1038/nn.3185.
Reprints and permissions information is available online at http://www.nature.com/reprints/index.html.

1. Bromberg-Martin, E.S., Matsumoto, M. & Hikosaka, O. Dopamine in motivational control: rewarding, aversive and alerting. *Neuron* **68**, 815–834 (2010).
2. Schultz, W. Multiple dopamine functions at different time courses. *Annu. Rev. Neurosci.* **30**, 259–288 (2007).
3. Lammel, S. *et al.* Unique properties of mesoprefrontal neurons within a dual mesocorticolimbic dopamine system. *Neuron* **57**, 760–773 (2008).
4. Lammel, S., Ion, D.I., Roeper, J. & Malenka, R.C. Projection-specific modulation of dopamine neuron synapses by aversive and rewarding stimuli. *Neuron* **70**, 855–862 (2011).
5. Krebs, R.M., Heipertz, D., Schuetze, H. & Duzel, E. Novelty increases the mesolimbic functional connectivity of the substantia nigra/ventral tegmental area (SN/VTA) during reward anticipation: Evidence from high-resolution fMRI. *Neuroimage* **58**, 647–655 (2011).
6. Jin, X. & Costa, R.M. Start/stop signals emerge in nigrostriatal circuits during sequence learning. *Nature* **466**, 457–462 (2010).
7. Zweifel, L.S. *et al.* Disruption of NMDAR-dependent burst firing by dopamine neurons provides selective assessment of phasic dopamine-dependent behavior. *Proc. Natl. Acad. Sci. USA* **106**, 7281–7288 (2009).
8. Brazhnik, E., Shah, F. & Tepper, J.M. GABAergic afferents activate both GABAA and GABAB receptors in mouse substantia nigra dopaminergic neurons *in vivo*. *J. Neurosci.* **28**, 10386–10398 (2008).
9. Johnson, S.W., Seutin, V. & North, R.A. Burst firing in dopamine neurons induced by *N*-methyl-D-aspartate: role of electrogenic sodium pump. *Science* **258**, 665–667 (1992).
10. Shen, K.Z. & Johnson, S.W. $Ca2^{+}$ influx through NMDA-gated channels activates ATP-sensitive K^{+} currents through a nitric oxide-cGMP pathway in subthalamic neurons. *J. Neurosci.* **30**, 1882–1893 (2010).
11. Gomis, A. & Valdeolmillos, M. Regulation by tolbutamide and diazoxide of the electrical activity in mouse pancreatic beta-cells recorded *in vivo*. *Br. J. Pharmacol.* **123**, 443–448 (1998).
12. Fridlyand, L.E., Tamarina, N. & Philipson, L.H. Bursting and calcium oscillations in pancreatic beta-cells: specific pacemakers for specific mechanisms. *Am. J. Physiol. Endocrinol. Metab.* **299**, E517–E532 (2010).
13. Liss, B., Bruns, R. & Roeper, J. Alternative sulfonylurea receptor expression defines metabolic sensitivity of K-ATP channels in dopaminergic midbrain neurons. *EMBO J.* **18**, 833–846 (1999).
14. Liss, B. *et al.* K-ATP channels promote the differential degeneration of dopaminergic midbrain neurons. *Nat. Neurosci.* **8**, 1742–1751 (2005).
15. Chan, C.S. *et al.* 'Rejuvenation' protects neurons in mouse models of Parkinson's disease. *Nature* **447**, 1081–1086 (2007).
16. Yamada, T., McGeer, P.L., Baimbridge, K.G. & McGeer, E.G. Relative sparing in Parkinson's disease of substantia nigra dopamine neurons containing calbindin-D28K. *Brain Res.* **526**, 303–307 (1990).
17. Grace, A.A. & Bunney, B.S. The control of firing pattern in nigral dopamine neurons: burst firing. *J. Neurosci.* **4**, 2877–2890 (1984).
18. Wilson, C.J., Young, S.J. & Groves, P.M. Statistical properties of neuronal spike trains in the substantia nigra: cell types and their interactions. *Brain Res.* **136**, 243–260 (1977).
19. Bingmer, M., Schiemann, J., Roeper, J. & Schneider, G. Measuring burstiness and regularity in oscillatory spike trains. *J. Neurosci. Methods* **201**, 426–437 (2011).
20. Yamada, K. *et al.* Protective role of ATP-sensitive potassium channels in hypoxia-induced generalized seizure. *Science* **292**, 1543–1546 (2001).
21. Dabrowski, M., Larsen, T., Ashcroft, F.M., Bondo Hansen, J. & Wahl, P. Potent and selective activation of the pancreatic beta-cell type K(ATP) channel by two novel diazoxide analogues. *Diabetologia* **46**, 1375–1382 (2003).
22. Zerangue, N., Schwappach, B., Jan, Y.N. & Jan, L.Y. A new ER trafficking signal regulates the subunit stoichiometry of plasma membrane K(ATP) channels. *Neuron* **22**, 537–548 (1999).
23. Bayer, H.M., Lau, B. & Glimcher, P.W. Statistics of midbrain dopamine neuron spike trains in the awake primate. *J. Neurophysiol.* **98**, 1428–1439 (2007).
24. Hyland, B.I., Reynolds, J.N., Hay, J., Perk, C.G. & Miller, R. Firing modes of midbrain dopamine cells in the freely moving rat. *Neuroscience* **114**, 475–492 (2002).
25. Deacon, R.M. *et al.* Behavioral phenotyping of mice lacking the K ATP channel subunit Kir6.2. *Physiol. Behav.* **87**, 723–733 (2006).
26. Gründemann, J., Schlaudraff, F., Haeckel, O. & Liss, B. Elevated alpha-synuclein mRNA levels in individual UV-laser-microdissected dopaminergic substantia nigra neurons in idiopathic Parkinson's disease. *Nucleic Acids Res.* **36**, e38 (2008).
27. Zaghloul, K.A. *et al.* Human substantia nigra neurons encode unexpected financial rewards. *Science* **323**, 1496–1499 (2009).
28. Nichols, C.G. KATP channels as molecular sensors of cellular metabolism. *Nature* **440**, 470–476 (2006).
29. Geng, X. *et al.* {alpha}-Synuclein binds the KATP channel at insulin-secretory granules and inhibits insulin secretion. *Am. J. Physiol. Endocrinol. Metab.* **300**, E276–E286 (2011).
30. Deister, C.A., Teagarden, M.A., Wilson, C.J. & Paladini, C.A. An intrinsic neuronal oscillator underlies dopaminergic neuron bursting. *J. Neurosci.* **29**, 15888–15897 (2009).
31. Johnson, S.W., Mercuri, N.B. & North, R.A. 5-hydroxytryptamine1B receptors block the GABAB synaptic potential in rat dopamine neurons. *J. Neurosci.* **12**, 2000–2006 (1992).
32. Parker, J.G., Beutler, L.R. & Palmiter, R.D. The contribution of NMDA receptor signaling in the corticobasal ganglia reward network to appetitive Pavlovian learning. *J. Neurosci.* **31**, 11362–11369 (2011).
33. Mameli-Engvall, M. *et al.* Hierarchical control of dopamine neuron-firing patterns by nicotinic receptors. *Neuron* **50**, 911–921 (2006).
34. Harnett, M.T., Bernier, B.E., Ahn, K.C. & Morikawa, H. Burst timing–dependent plasticity of NMDA receptor-mediated transmission in midbrain dopamine neurons. *Neuron* **62**, 826–838 (2009).
35. Herrik, K.F., Christophersen, P. & Shepard, P.D. Pharmacological modulation of the gating properties of small conductance $Ca2^{+}$-activated K^{+} channels alters the firing pattern of dopamine neurons *in vivo*. *J. Neurophysiol.* **104**, 1726–1735 (2010).
36. Opland, D.M., Leinninger, G.M. & Myers, M.G. Jr. Modulation of the mesolimbic dopamine system by leptin. *Brain Res.* **1350**, 65–70 (2010).
37. Andrews, Z.B. *et al.* Ghrelin promotes and protects nigrostriatal dopamine function via a UCP2-dependent mitochondrial mechanism. *J. Neurosci.* **29**, 14057–14065 (2009).
38. Haber, S.N. & Knutson, B. The reward circuit: linking primate anatomy and human imaging. *Neuropsychopharmacology* **35**, 4–26 (2010).
39. Kravitz, A.V. *et al.* Regulation of parkinsonian motor behaviours by optogenetic control of basal ganglia circuitry. *Nature* **466**, 622–626 (2010).
40. Lex, B. & Hauber, W. The role of dopamine in the prelimbic cortex and the dorsomedial striatum in instrumental conditioning. *Cereb. Cortex* **20**, 873–883 (2010).
41. Lex, B. & Hauber, W. Disconnection of the entorhinal cortex and dorsomedial striatum impairs the sensitivity to instrumental contingency degradation. *Neuropsychopharmacology* **35**, 1788–1796 (2010).
42. Lisman, J.E. & Grace, A.A. The hippocampal-VTA loop: controlling the entry of information into long-term memory. *Neuron* **46**, 703–713 (2005).
43. Bunzeck, N. & Duzel, E. Absolute coding of stimulus novelty in the human substantia nigra/VTA. *Neuron* **51**, 369–379 (2006).
44. Bódi, N. *et al.* Reward-learning and the novelty-seeking personality: a between- and within-subjects study of the effects of dopamine agonists on young Parkinson's patients. *Brain* **132**, 2385–2395 (2009).
45. Rutledge, R.B. *et al.* Dopaminergic drugs modulate learning rates and perseveration in Parkinson's patients in a dynamic foraging task. *J. Neurosci.* **29**, 15104–15114 (2009).
46. Guzman, J.N. *et al.* Oxidant stress evoked by pacemaking in dopaminergic neurons is attenuated by DJ-1. *Nature* **468**, 696–700 (2010).
47. Ungless, M.A., Magill, P.J. & Bolam, J.P. Uniform inhibition of dopamine neurons in the ventral tegmental area by aversive stimuli. *Science* **303**, 2040–2042 (2004).
48. Franklin, K. & Paxinos, G. *The Mouse Brain in Stereotaxic Coordinates* (Elsevier, 2001).

ONLINE METHODS

Animals. Experiments were performed on adult (10–16 weeks old) male C57bl6N and *Kir6.2*$^{-/-}$ (backcrossed into C57bl6 mice[14]) mice housed in groups on a 12-h light-dark cycle. Procedures approved by the Regierungspräsidium Gießen and Darmstadt (V54-19c20/15-F28/07, -F40/28).

Extracellular *in vivo* single-unit recordings. For *in vivo* electrophysiology, mice (0.1 mg per kg of body weight atropine, 1 g per kg glucose in H_2O, subcutaneous before recording) were anesthetized with isoflurane (0.8–1.4% in O_2, 0.35 l min^{-1}; lidocaine gel for local analgesia) and placed in a stereotaxic frame (Kopf). Rectal temperature (33–36 °C), heart rate (5–7 Hz), respiration (1–2 Hz) and electrocorticograms were constantly monitored. Electrocorticograms recordings with 1-mm stainless steel screw above left cortex (*x*, 1.2 mm lateral; *y*, 2.1 mm anterior of bregma) referred to screw above ipsilateral cerebellum (*x*, 1.2; *y*, −5.5 to −6.5 mm)[49].

Craniotomies and recording depth were at the following coordinates[48] (lateral (*x*), posterior (*y*), ventral (*z*) to bregma, in mm): m-SN (0.8, −3.08, 3.7–4.4), l-SN (1.2, −3.08, 3.7–4.2) and VTA (0.1–0.4, −3.6, 3.5–4.3). *y* coordinates adjusted to skull size (in mm, *y* = −3.08/4.2*distance(bregma − lambda) + 0.2). Electrodes were moved using a micromanipulator (SM-6, Luigs and Neumann). Single-units recorded for >10 min using glass microelectrodes (resistance 15-25MΩ; Harvard Apparatus) filled with 0.5 M NaCl, 10 mM HEPES and 1.5% neurobiotin (wt/vol) (Vector Laboratories). Signals were amplified 1,000× (ELC-03M, NPI Electronics), notch and band-pass filtered 50Hz-5kHz (single-pole, 6 dB per octave, DPA-2FS, NPI Electronics), acquired with a EPC-10 A/D converter (PatchMaster software, Heka; sampling rate 12.5 kHz for spike trains, 20 kHz for action potential waveforms), and displayed on an analog oscilloscope and audiomonitor. DA neurons were electrophysiologically identified by broad triphasic action potentials (≥1.1 ms)[47] with single spike-oscillatory/irregular or bursty-oscillatory/irregular spontaneous spiking (frequency range of 0.5–10 Hz, classical 80/160-ms criterion for burst detection[17]. Data were analyzed with IgorPro6.02 (WaveMetrics), Spike2 (6.11, Cambridge Electronic Design), R statistical computing (http://www.r-project.org/), CVI5.01 (National Instruments) and NeuroExplorer4 (Nex Technologies) software.

Juxtacellular labeling and immunohistochemical characterization of recorded neurons. After *in vivo* recording, single neurons were labeled with neurobiotin using the juxtacellular technique[50]. Positive current pulses (1–10 nA, 200 ms on/off pulses) were applied with continuous monitoring of activity. Labeling was successful if modulation of activity was stable for >25–300 s and discharges continued after modulation. Single-cell labeling allowed to map localization of recorded neurons in DA subnuclei and to identify their neurochemical phenotype using tyrosine hydroxylase and calbindin-D28K immunostaining.

Multi-labeling immunocytochemistry and confocal analyses. Anesthetized animals (sodium pentobarbital, 1.6 g per kg) were transcardially perfused with 4% paraformaldehyde (wt/vol) and 15% picric acid (vol/vol) in phosphate-buffered saline (PBS, pH 7.4). Brains were post-fixed overnight and coronal midbrain sections (60 µm) were prepared. Sections were incubated in blocking solution (0.01 M PBS, 10% horse serum (vol/vol), 0.5% Triton X-100 (vol/vol), 0.2% BSA (vol/vol)). For primary antibodies, we used polyclonal rabbit antibody to tyrosine hydroxylase (catalog no. 657012,1:1,000, Calbiochem), monoclonal mouse antibody to calbindin-D28K (1:750, catalog no. 300, Swant), monoclonal mouse antibody to GABA (1:500, catalog no. A0310, Sigma) and monoclonal mouse antibody to HA.11 (1:1,000, clone 16B12, Covance), diluted in carrier solution (0.01 M PBS, 1% horse serum, 0.5% Triton X-100, 0.2% BSA, 22 °C, overnight). We used streptavidin-488 (catalog no. S11223) or streptavidin-568 (catalog no. S11226), 1:1,000, Molecular Probes), and AlexaFluor-568 (catalog no. A-11036) or AlexaFluor-647 goat antibodies to rabbit (catalog no. A-21245) and AlexaFluor-488 (catalog no. A-11001), AlexaFluor-568 (catalog no. A-11004) or AlexaFluor-647 goat antibodies to mouse (catalog no. A-21236, all 1:750, Molecular Probes) as secondary antibodies (in carrier solution, 22 °C, overnight). Sections were mounted on slides (Vectashield, Vector). For confocal analyses, multi-labeling fluorescent immunostaining of juxtacellularly filled neurons were analyzed with a laser-scanning microscope (LSM510 Meta, Zeitz) using either a 10×/0.3 or 63×/1.4 oil lens (2× zoom). Identical confocal settings were chosen for all scanned neurons. 3,3′-diaminobenzidine staining was carried out using biotinylated goat antibody to rabbit as a secondary antibody (catalog no. BA-1000, 1:1,000) and the Vectastain ABC kit, sections were mounted on slides (Vectamount, Vector) and documented with light microscopy.

ACH-based classification of firing patterns. Autocorrelation histograms were plotted using R (1-ms bins, smoothed with Gaussian filter (20 ms)). We used established criteria for classification of *in vivo* firing patterns based on visual inspection of autocorrelograms[18]: single spike-oscillatory (≥3 equidistant peaks with decreasing amplitudes), single spike-irregular (<3 peaks, increasing from zero approximating a steady state), bursty-irregular (narrow peak with steep increase at short ISIs) and bursty-oscillatory (narrow peak reflecting fast intraburst ISIs followed by clear trough and repetitive broader peaks)[51]. For GLO-based classification of firing patterns see ref. 19 and **Supplementary Note**.

Stereotaxically guided rAAV2-mediated gene expression in SN DA neurons *in vivo*. Viral dominant-negative Kir6.2 pore-mutant (Kir6.2_DN) constructs carried a point mutation in the selectivity filter (Gly132Ser) that disrupts conductance of K-ATP channels[52]. Kir6.2_DN: rAAV2-SAR-CAG-murineKir6.2_G132S_HA-WPRE-BGH-polyA, titer of 1.3×10^{10} genomic particles per ml for electrophysiology and behavior experiments. Vectors expressing native Kir6.2 subunits (Kir6.2_WT) were used as control. Kir6.2_WT: rAAV2-SAR-CAG-murineKir6.2_WT_HA-WPRE-BGH-polyA (1.2×10^{10} genomic particles per ml). rAAV2 expression constructs were produced by GeneDetect. Stereotaxic operation procedures for rAAV2 injections were performed similar to *in vivo* recordings. Virus solutions (diluted in artificial cerebrospinal fluid (ACSF), Harvard Apparatus) were infused bilaterally into the SN at medial (in mm: *x*, 0.8; *y*, −3.03; *z*, 4.0; 1.8 µl) and/or a lateral (*x*, 1.4; *y*, −3.18; *z*, 3.7; 1.1 µl, 100 nl min^{-1}) sites using a micro-pump (UMP3-1, WPI). Although selective injections into the l-SN did not spread into more medial regions, selective injections into m-SN showed transduction in l-SN. Thus, selective targeting of only the m-SN was not possible. Behavior was tested on post-operative days 13–14 and *in vitro* or *in vivo* recordings were carried out on days 14–15.

Immunohistochemical verification of rAAV2-mediated transgene expression and identification of transduced, electrophysiologically recorded neurons was performed as described above (mouse antibody to HA.11). For quantification of transduction efficiency and selectivity, tyrosine hydroxylase– and HA-immunopositive neurons were counted using confocal images (40×/1.3 oil objective, LSM510 Meta, Zeitz) throughout the medial-lateral and rostral-caudal extent of SN and VTA (*N* = 6 mice).

We probed for synaptic uptake and retrograde transport of rAAV2 constructs[53,54] (**Supplementary Fig. 6**). Coronal sections (100 µm) of brains injected unilaterally with Kir6.2_DN (right m-SN/l-SN, non-injected site as control, *N* = 3 mice) were prepared. Sections were processed for tyrosine hydroxylase and HA immunohistochemistry and counterstained using nissl red 530 nm (Invitrogen, Life Technologies; 1:1,000 in PBS, incubated for 20 min, rinsed in PBS for >2 h and mounted on slides).

To test anterograde transport of Kir6.2_DN back to synaptic terminals on SN DA neurons, we combined stereotaxic Kir6.2_DN injections with multiple immunofluorescent labeling of synaptic terminals (as above, with 10% and 1% goat instead of horse serum). To investigate co-localization of HA-tagged viral transgene with synapse marker proteins in terminals on tyrosine hydroxylase and HA double-positive SN DA neurons, we used the following polyclonal primary antibodies: rabbit antibody to synapsin1 (catalog no. 106 103), guinea pig antibody to vesicular GABA transporter (VGAT, catalog no. 131 004), guinea pig antibody to vesicular glutamate transporter 1 (VGLUT1, catalog no. 135 304), guinea pig antibody to vesicular glutamate transporter 2 (VGLUT2, catalog no. 135 404, all 1:1,000, SynapticSystems), rabbit antibody to tyrosine hydroxylase (1:1,000; catalog no. 657012, Calbiochem) and monoclonal mouse antibody to HA.11 (1:1,000; clone 16B12, Covance). These were combined with highly cross-absorbed secondary antibodies: AlexaFluor-568 goat antibody to guinea pig (catalog no. A-11075), AlexaFluor-647 goat antibody to rabbit (catalog no. A-21450), AlexaFluor-488 goat antibody to mouse (catalog no. A-11073, all 1:750, Molecular Probes). Control experiments to test antibody specificity of Synapsin1, VGAT, VGLUT1 and VLGUT2 included omission of primary antibodies and pre-absorption with corresponding control peptides (SynapticSystems, all experiments used 40-µm coronal midbrain sections).

Images were taken with a confocal laser-scanning microscope (LSM510 Meta, Zeitz; 63×/1.4 oil DIC lens (4× zoom, 56–69-µm pinhole, <0.6-µm

optical slice))[55]. Identical settings for all images, 10–15 neurons scanned per injection site ($n = 4$, $N = 3$ animals). VGAT-, VGLUT1- or VGLUT2-positive structures without spatial separation from surface of HA and tyrosine hydroxylase double-positive somata (scanned at plane of nucleus) were recognized as putative synapses (**Supplementary Fig. 6b**). Synaptic localization of viral HA-tag and its co-expression with VGAT, VGLUT1 and VGLUT2 was quantitatively analyzed.

For further control experiments (**Supplementary Fig. 5**), we also studied rAAV2 vectors without transgene expression and eGFP-expressing constructs[56]. Empty vector: rAAV2-SAR-CAG-empty/null-WPRE-BGH-polyA (1.1×10^{12} genomic particles per ml). eGFP vector: rAAV2-SAR-CAG-eGFP-WPRE-BGH-polyA (1.1×10^{12} genomic particles per ml, used for *in vivo* recordings, 6–7 d post infusion).

***In vitro* patch-clamp recordings in adult brain slices.** Coronal midbrain slices of adult mice were sectioned (250 µm) after intracardial perfusion using ice-cold ACSF (50 mM sucrose, 125 mM NaCl, 2.5 mM KCl, 25 mM $NaHCO_3$, 1.25 mM NaH_2PO_4, 2.5 mM glucose, 6.2 mM $MgCl_2$, 0.1 mM $CaCl_2$ and 2.96 mM kynurenic acid (Sigma), oxygenated with 95%O_2/5%CO_2). Slices were transferred to recording chamber after ≥90 min and continuously perfused with oxygenated ACSF (2–4 ml min^{-1}, 36 °C; 22.5 mM sucrose, 125 mM NaCl, 2.5 mM KCl, 25 mM $NaHCO_3$, 1.25 mM NaH_2PO_4, 2.5 mM glucose, 2.1 mM $MgCl_2$ and 2 mM $CaCl_2$; 95% O_2/5% CO_2). CNQX (12.5 µM; Biotrend) and gabazine (SR95531, 4 µM; Biotrend) were added to inhibit fast excitatory and inhibitory synaptic transmission, respectively. ATP washout experiments were carried out in whole-cell configuration using patch pipettes (3–4.5 MΩ) containing 20 mM NaCl, 140 mM KCl, 10 mM HEPES, 0.1 mM EGTA, 2 mM $MgCl_2$ and 0.1% neurobiotin (pH 7.4, 275 mOsm). K-ATP currents were elicited with a ramp protocol (−120 mV to −30 mV, 200 ms) from a holding potential of −50 mV. Somatic on-cell recordings were carried out with higher pipette resistance (8–12 MΩ; 140 mM KCl, 10 mM HEPES, 0.1 mM EGTA and 2 mM $MgCl_2$). For NMDA-mediated burst induction, 10 µM gabazine, 20 µM CNQX were used and D2 and GABA-B receptors were inhibited by 1 µM sulpiride (Tocris Bioscience) and 1 µM CGP55845 (Tocris), respectively. ACSF contained 3.5 mM KCl and 1 mM lactate. 300 µM tolbutamide (Sigma), 10 µM NN414 (Axon Medchem) and 30 µM NMDA (Sigma) were bath applied.

SN DA neurons were visualized by video microscopy, recordings were performed in voltage-clamp using an EPC-10 patch amplifier (HeKa) with a sampling rate of 10 kHz (low-pass filter, 5 kHz). Analyses were carried out in FitMaster (HeKa) and IgorPro (WaveMetrics).

Behavioral testing. Spontaneous locomotor and exploratory activity (track length, wall distance, time in center and number of rearings) of wild-type, *Kir6.2*$^{-/-}$ and virus-injected animals (handled for 2 d) were analyzed in open field (50 × 50 cm, center 30 × 30 cm; red illumination, 3 lx) for 20 min using a video tracking system (Viewer II, Biobserve; rearings were analyzed via beam breaks, height 4.5 cm). The open field was novel to all animals on day 1 (open field 1, forced novelty), and wild type and *Kir6.2*$^{-/-}$ were also tested on consecutive day 2. Unpaired *t* tests were used to compare activity in different phases (initial, 1–2 min; steady state, 3–20 min).

UV-LMD and quantitative real-time PCR of human DA midbrain neurons from Parkinson's disease patients and controls. mRNA levels were analyzed in pools of 15 individual neuromelanin-positive SN DA neurons from ethanol-fixed, cresyl violet–stained, horizontal midbrain cryosections of human post-mortem Parkinson's disease and matched control brains (German BrainNet) via UV-LMD and quantitative reverse-transcription PCR essentially as described[57]. RNA integrity number and pH of all brains were assessed. Ten neuron pools were collected for each brain. Only pools positive for tyrosine hydroxylase were included. mRNA levels per cell are given as picogram equivalents of total cDNA derived from human SN control tissue RNA (Ambion, Applied Biosystems), determined via quantitative real-time PCR and standard curve quantification. See **Supplementary Table 4b** for human TaqMan Assay IDs (Applied Biosystems, Life Technologies), human cDNA standard curve parameters and fluorescence thresholds for Ct and data analysis.

Analysis of putative SN DA neurons in Parkinson's disease patients. *In vivo* electrophysiological recordings of SN DA neurons in Parkinson's disease patients undergoing deep brain stimulation surgery are taken from a published data set[27] and were reanalyzed identical to our mouse data set. On the basis of mean rate and stationarity, 13 of 15 of the putative SN DA neurons were selected for analysis.

Statistical analyses. Kolmogorov-Smirnov normality tests and Levene tests for equal variances (for confirmation of test assumptions), Student`s paired or unpaired *t* tests (two tailed), Mann-Whitney U tests (two tailed), Wilcoxon-rank tests, one-way ANOVA (with Bonferroni *post hoc* tests) as annotated for each comparison were calculated using SPSS18.0 (PASW, IBM) or GraphPad Prism 5.0c software. Graphs were plotted with GraphPad. The distributions of electrophysiological patterns were analyzed with R statistical computing using a Pearson's Chi-squared test statistic (based on 10^6 permutations). In the case of significant results, individual tests were performed using Fisher's Exact test for each category, pooling the counts in the remaining categories (also, for analyses of overall burstiness regular-bursty and irregular-bursty patterns were pooled, except for data presented in **Supplementary Fig. 1** and **Supplementary Table 1**). Resulting *P* values were compared to Bonferroni-corrected α-level.

49. Brown, M.T., Henny, P., Bolam, J.P. & Magill, P.J. Activity of neurochemically heterogeneous dopaminergic neurons in the substantia nigra during spontaneous and driven changes in brain state. *J. Neurosci.* **29**, 2915–2925 (2009).
50. Pinault, D. A novel single-cell staining procedure performed *in vivo* under electrophysiological control: morpho-functional features of juxtacellularly labeled thalamic cells and other central neurons with biocytin or Neurobiotin. *J. Neurosci. Methods* **65**, 113–136 (1996).
51. Zhang, D., Yang, S., Jin, G.Z., Bunney, B.S. & Shi, W.X. Oscillatory firing of dopamine neurons: differences between cells in the substantia nigra and ventral tegmental area. *Synapse* **62**, 169–175 (2008).
52. Miki, T. *et al.* Abnormalities of pancreatic islets by targeted expression of a dominant-negative KATP channel. *Proc. Natl. Acad. Sci. USA* **94**, 11969–11973 (1997).
53. Burger, C. *et al.* Recombinant AAV viral vectors pseudotyped with viral capsids from serotypes 1, 2 and 5 display differential efficiency and cell tropism after delivery to different regions of the central nervous system. *Mol. Ther.* **10**, 302–317 (2004).
54. Henny, P. *et al.* Structural correlates of heterogeneous *in vivo* activity of midbrain dopaminergic neurons. *Nat. Neurosci.* **15**, 613–619 (2012).
55. Martín-Ibañez, R. *et al.* Vesicular glutamate transporter 3 (VGLUT3) identifies spatially segregated excitatory terminals in the rat substantia nigra. *Eur. J. Neurosci.* **23**, 1063–1070 (2006).
56. Ulusoy, A., Sahin, G., Bjorklund, T., Aebischer, P. & Kirik, D. Dose optimization for long-term rAAV-mediated RNA interference in the nigrostriatal projection neurons. *Mol. Ther.* **17**, 1574–1584 (2009).
57. Gründemann, J., Schlaudraff, F. & Liss, B. UV-laser microdissection and mRNA expression analysis of individual neurons from postmortem Parkinson's disease brains. *Methods Mol. Biol.* **755**, 363–374 (2011).

doi:10.1038/nn.3185